GA–A24407

SAFETY FACTOR SCALING OF ENERGY TRANSPORT IN L–MODE PLASMAS ON THE DIII–D TOKAMAK

by
C.C. PETTY, J.E. KINSEY, and T.C. LUCE

SEPTEMBER 2003

DISCLAIMER

GA–A24407

SAFETY FACTOR SCALING OF ENERGY TRANSPORT IN L–MODE PLASMAS ON THE DIII–D TOKAMAK

by
C.C. PETTY, J.E. KINSEY,* and T.C. LUCE

This is a preprint of a paper to be submitted for publication in *Phys. Plasmas.*

*Lehigh University, Bethlehem, Pennsylvania.

Work supported by
the U.S. Department of Energy under
Contract No. DE-AC03-99ER54463 and
Grant No. DE-FG02-92ER54141

GENERAL ATOMICS PROJECT 30033
SEPTEMBER 2003

Abstract

The scaling of energy transport with safety factor (q) at fixed magnetic shear has been measured on the DIII-D tokamak [Nucl. Fusion **42**, 614 (2002)] for low confinement (L) mode discharges. At constant density, temperature, and toroidal magnetic field strength, such that the toroidal dimensionless parameters other than q are held fixed, the one-fluid thermal diffusivity is found to scale like $\chi \propto q^{0.84\pm0.15}$, with the ion channel having a stronger q dependence than the electron channel in the outer half of the plasma. The measured q scaling is in good agreement with the predicted scaling by the GLF23 transport model for the ion temperature gradient and trapped electron modes, but it is significantly weaker than the inferred scaling from empirically-derived confinement scaling relations.

I. INTRODUCTION

Dimensional analysis, along with the related methods of similarity and scale invariance, is a powerful technique for analyzing physical systems [1–3]. While dimensionless parameter scaling has been a standard tool in both theoretical and experimental physics for many years [4], it has only been over the last dozen years that significant progress has been made towards predicting and understanding radial energy transport in fusion plasmas using this technique. In fact, it has only recently been verified that tokamak plasmas with widely different physical parameters (including size) but identical dimensionless parameters have the same normalized energy transport, *i.e.*, they exhibit similarity [5]. Most of the dimensionless parameter scaling experiments to date have concentrated on measuring the scaling of energy transport with relative gyroradius [6–18] (ρ_*), although the scaling with beta [10,19–21] (β) and collisionality [10,16,17,19,20,22] (ν) have also been reported. In this paper, the safety factor (q) scaling of energy transport in low confinement (L) mode plasmas on the DIII-D tokamak [23] is measured for the first time with all of the other dimensionless parameters held fixed, including the magnetic shear (the q scaling of high confinement (H) mode plasmas on DIII-D was reported previously [24]). The experimental q scaling of energy transport is also compared with theory-based modeling in this paper to help validate the proposed instability mechanisms.

If radial energy transport is governed only by the Boltzmann and Maxwell equations, then Connor-Taylor scale invariance arguments [2] lead to a thermal diffusivity (χ) that is dependent only upon the local dimensionless quantities,

$$\frac{\chi}{\chi_B} = F\left(q, \rho_*, \beta, \nu, \epsilon, \ldots\right) \quad , \tag{1}$$

where the functional form of F cannot be easily estimated from theory. In this equation, $\chi_B \sim T/eB_T$ is the Bohm diffusion coefficient, $q \sim \epsilon B_T/B_p$ is the safety factor, $\rho_* \sim \sqrt{T}/aB_T$, $\beta \sim nT/B_T^2$, $\nu \sim na/T^2$, e is the charge of an electron, a is the plasma minor radius, ϵ is the inverse aspect ratio, n is the plasma density, T is the plasma temperature, and B_p and B_T are the poloidal and toroidal magnetic field strengths. It is usually assumed that the transport dependencies on the various dimensionless variables can be separated; therefore, the scaling of energy transport with the safety factor can be written in the form

$$\frac{\chi}{\chi_B} = q^{\alpha_q}\, G\left(\rho_*, \beta, \nu, \epsilon, \ldots\right) \quad . \tag{2}$$

This type of power law dependence for q is actually not expected in general since the safety factor affects not only the linear growth rate of the mode but also the critical

gradient for the mode onset [25]. However, experimentally it is difficult to determine a more complicated scaling than this, and it is convenient for later comparison with empirically-derived confinement scaling relations based upon physical parameters. Varying q while keeping the other dimensionless quantities (ρ_*, β, ν, *etc.*) fixed allows the exponent α_q from Eq. (2) to be determined from the measured change in the thermal diffusivity since the unspecified function G remains constant. Of course, if a different set of dimensionless parameters is specified in the function G in Eq. (2), then the value of the exponent α_q will likely change. However, since the Buckingham Π theorem [4] allows the specific form of any dimensionless parameter to be replaced by any function of itself (because this function will also be dimensionless and independent of the remaining parameters), the change in the value of α_q will be uniquely determined by the transformation of variables.

Drift wave models of turbulent transport [26] generally predict a dependence of transport on the safety factor in the range of $\chi \propto q^{1-2}$. For example, the toroidal ion temperature gradient (ITG) mode and trapped electron mode exhibit an approximately linear increase in transport with increasing safety factor, owing to a downshift of the spectral weight to long perpendicular wavelengths as well as a change in the turbulence growth rates [27]. Models of the resistive ballooning mode [28], which is predicted to be important only in the plasma edge, have a robust transport scaling like $\chi \propto q^2$. These theoretical dependences refer to the simplified case where the stabilizations from the Shafranov shift and $E \times B$ shear do not vary with q, which is not the situation for the DIII-D experiments discussed in this paper. For plasmas that are rotating toroidally owing to unbalanced neutral beam injection (NBI) and have a small pressure gradient contribution to the radial electric field, the normalized rotational shearing rate is inversely proportional to the safety factor at fixed Mach number,

$$\frac{\gamma_{E\times B}}{\gamma_{\max}} \sim \left| \frac{(RB_p/B_T)\nabla(V_T/R)}{c_s/R} \right| \sim \left| \frac{M_T}{q} \right| \quad , \tag{3}$$

where $\gamma_{E\times B}$ is the $E \times B$ velocity shearing rate, $\gamma_{\max}$ is the linear growth rate of the fastest growing mode involved in the transport (assumed independent of q), R is the plasma major radius, V_T is the toroidal rotational velocity of the ions, c_s is the ion sound velocity, and $M_T = V_T/c_s$ is the toroidal Mach number. Therefore, $E \times B$ shear acts to strengthen the apparent q scaling of transport.

The rest of this paper is organized as follows: Sec. II describes the DIII-D tokamak and the plasma diagnostics used in these experiments. Results from the safety factor scaling experiments in L-mode plasmas are reported in Sec. III, and are compared to predictions from theory-based transport modeling in Sec. IV. In Sec. V, a comparison is given between the DIII-D dimensionless parameter scaling studies and the physical

parameter scalings from L-mode confinement scaling relations. The conclusions are presented in Sec. VI.

II. EXPERIMENTAL SETUP

For these transport experiments on the DIII-D tokamak, a double null divertor plasma shape is biassed vertically with the dominant X point opposite the ∇B drift direction to keep the plasma in L mode. The plasma configurations for the low-q and high-q discharges studied in this paper are displayed in Fig. 1. These discharges have a major radius of $R = 1.66$ m, a minor radius of $a = 0.63$ m, an elongation of $\kappa = 1.5$, and an average triangularity of $\delta = 0.5$. The primary ion species is deuterium, with carbon being the dominant impurity species. Deuterium NBI is used for auxiliary heating, and the vessel walls are boronized to reduce the impurity influx during NBI heating. Neutral beam heating is applied early during the plasma current (I) ramp up to keep q above unity and avoid sawteeth during the transport time of interest.

A number of diagnostics are utilized in the plasma equilibrium reconstruction and local transport analysis on DIII-D. The electron density (n_e) profile is measured using multi-pulse Thomson scattering [29] along with four CO_2 laser interferometers. The electron temperature (T_e) profile is found from a combination of Thomson scattering and electron cyclotron emission (ECE) measured with a Michelson interferometer [30]. The ion temperature (T_i) profile is determined from charge exchange recombination (CER) emission of carbon impurities [31]. The carbon density found from the CER emission also determines the average ion charge ($Z_{\rm eff}$) profile [32]. An array of foil bolometers is used to measure the radiated power ($P_{\rm rad}$) profile [33]. The plasma current and safety factor profiles are determined from an axisymmetric reconstruction of the magnetic equilibrium using the external magnetic measurements and the magnetic pitch angles measured using the motional Stark effect [34–36] (MSE).

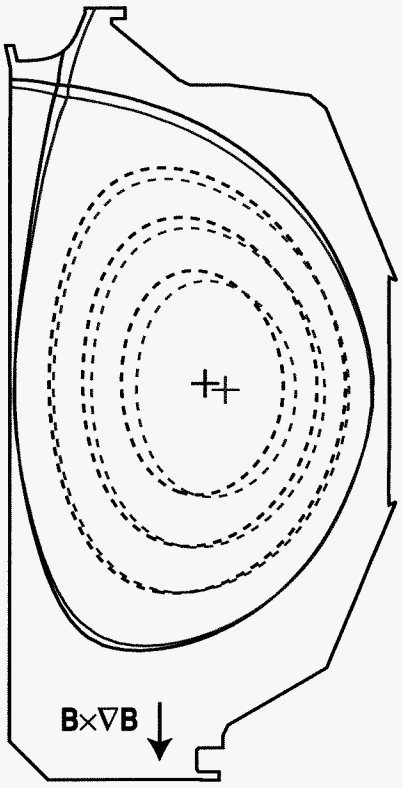

Fig. 1. Equilibrium reconstruction of the magnetic field contours and the plasma shape with respect to the vessel walls. The figure shows the low-q discharge (solid lines) superimposed on the high-q discharge (dashed lines).

III. SAFETY FACTOR SCALING OF ENERGY TRANSPORT

The safety factor scaling of the energy confinement time and local thermal diffusivity has been measured for L-mode plasmas on DIII-D by varying the plasma current at constant ρ_*, β, ν, and magnetic shear ($\hat{s} \equiv r\nabla q/q$). Although many tokamak experiments have measured the I scaling of confinement, this is usually done at fixed auxiliary heating power such that ρ_*, β and ν vary. Furthermore, since sawteeth usually fix the safety factor to a value near unity on axis, I scans normally vary the local values of both q and $\hat{s}$, complicating the interpretation. In these experiments, the q scan is done at fixed $\hat{s}$ by controlling the formation and evolution of the q profile during the initial phase of the discharge by adjusting the level and timing of the NBI heating [37], allowing the safety factor scaling of energy transport to be unambiguously determined. In order to keep ρ_*, β and ν constant during the safety factor scan, the plasma density, temperature and magnetic field strength are held fixed (if the plasma radius were to vary, then the quantities $Ba^{5/4}$, na^2 and $Ta^{1/2}$ would need to be held fixed). This means that the Bohm diffusion coefficient does not change during the safety factor scan, and the values of the thermal diffusivity and confinement time do not need to be normalized to χ_B to interpret the results. Turbulence measurements of these discharges found that the radial correlation lengths of density fluctuations scaled with the ion toroidal gyroradius rather than the ion poloidal gyroradius [38].

Table I shows that the global plasma parameters are well matched for a scan in the plasma current from 0.80 MA to 1.48 MA. The safety factor is varied by a multiplicative factor of 1.8 across its entire radial profile for these two L-mode discharges, as shown in Fig. 2, therefore the magnetic shear is nearly unchanged. The plasma density, thermal stored energy (W_{th}), and plasma shape (with the exception of δ) are matched to within 4% for the two different q discharges in Table I while the stored toroidal angular momentum (ℓ_{mom}) is matched to within 10%. Since the thermal plasma beta and plasma shape are held constant, the poloidal beta $\beta_p \sim nT/B_p^2$ varies significantly during the safety factor scan. Therefore, the high-q discharge has a greater Shafranov shift than the low-q discharge, as seen in Fig. 1.

TABLE I
PHYSICAL AND DIMENSIONLESS PARAMETERS FOR L-MODE SAFETY FACTOR SCALING EXPERIMENT AT FIXED MAGNETIC SHEAR

Parameter	#106748	#106740
I (MA)	0.80	1.48
B_T (T)	2.05	2.03
R (m)	1.66	1.66
a (m)	0.63	0.63
$\bar{n}$ (10^{19} m^{-3})	2.1	2.1
ℓ_{mom} (kg m^{2}s^{-1})	0.11	0.12
W_{th} (MJ)	0.155	0.160
P (MS)	5.2	3.5
τ_{th} (s)	0.030	0.046
τ_{mon} (s)	0.030	0.065
R/a	2.63	2.63
κ	1.53	1.577
δ	0.48	0.53
q_{95}	6.3	3.5
q_0	2.1	1.3
β^{th} (%)	0.33	0.34
β_p^{th}	0.36	0.11

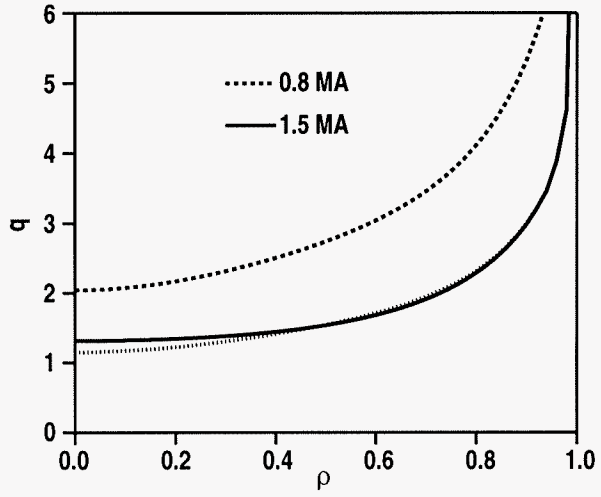

Fig. 2. Radial profiles of the safety factor from an equilibrium reconstruction constrained by MSE measurements for the 0.8 MA (dashed line) and 1.5 MA (solid line) discharges in Table I. The dotted line represents the 0.8 MA profile scaled down by a constant factor of 1.8.

The thermal energy confinement time is found to have a weaker than linear dependence on the safety factor for these L-mode discharges. Although the q profile is slowly evolving during the analysis time window owing to the relaxation of the parallel electric field, the relaxation time at constant current is much longer than the energy confinement time; therefore, $\dot{W}$ corrections to the heating power (P) are negligible (less than 3%). Table 1 shows that the thermal energy confinement time increases by a factor of 1.5 for a decrease in the safety factor by a factor of 1.8. This results in the thermal energy confinement time scaling like $\tau_{th} \propto q^{-0.8\pm0.1}$ at fixed $\hat{s}$ for L-mode plasmas, where the uncertainty in the q scaling exponent is due to the random error in measuring the plasma profiles. This q scaling of τ_{th} at fixed $\hat{s}$ is significantly weaker than for H-mode plasmas on DIII-D [24]. The q dependence of the momentum confinement time can be determined in an analogous fashion since the stored angular momentum is kept nearly constant by matching the toroidal Mach numbers. From Table I, the momentum confinement time is seen to have a stronger q scaling than the energy confinement, $\tau_{mom} \propto q^{-1.3\pm0.1}$.

In addition to the good match in the global parameters shown in Table I, the local values of the plasma parameters are also kept nearly fixed during the safety factor scan. The profiles of the electron and ion temperatures, the electron density, and the effective ion charge are shown in Fig. 3 as a function of the normalized toroidal flux coordinate (ρ). The largest mismatch is in the T_i profile near the plasma center, where the high-q plasma tends towards a hot ion mode. Otherwise, the plasma profiles are well matched for $0.3 \leq \rho \leq 1.0$, and the local energy transport analysis will be restricted to this region. A comparison of the radial profiles of the dimensionless parameters in Fig. 4 shows that these quantities are also matched between the high-q and low-q discharges. Note that the form of the collisionality that is held fixed in this experiment does not have any q dependence, *i.e.*, $\nu_i \sim \nu_{*i}/q$ where ν_{*i} is the ion collision frequency normalized to the ion bounce frequency. The largest mismatch in the dimensionless parameters is in the T_e/T_i ratio, which systematically varies by 13% in the region $0.3 \leq \rho \leq 0.9$ for the two L-mode plasmas. The mismatch in ρ_{*i} and M_T in the region $0.0 \leq \rho \leq 0.3$ is due to the hot ion mode feature in the high-q discharge mentioned previously. Figure 4 also verifies that the magnetic shear is kept nearly constant during the factor of 1.8 scan in the safety factor.

A local transport analysis finds that the thermal diffusivities have a slightly weaker than linear dependence on the safety factor across the entire plasma radius for these L-mode plasmas, the magnitude of which is in agreement with the scaling of the thermal energy confinement time. The radial power balance equation is solved in the experimental magnetic geometry by the ONETWO transport code [39], which

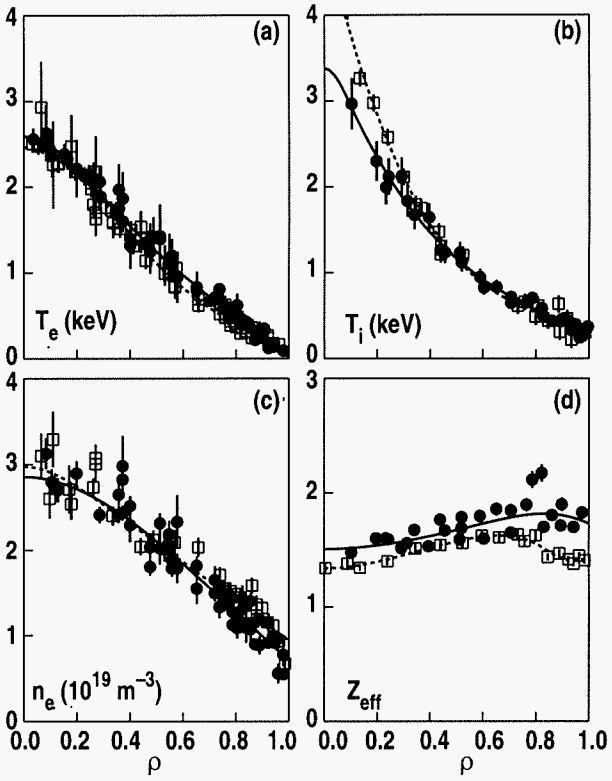

Fig. 3. Radial profiles of (a) electron temperature, (b) ion temperature, (c) electron density, and (d) effective ion charge for the 0.8 MA (open squares and dashed lines) and 1.5 MA (filled circles and solid lines) L-mode discharges.

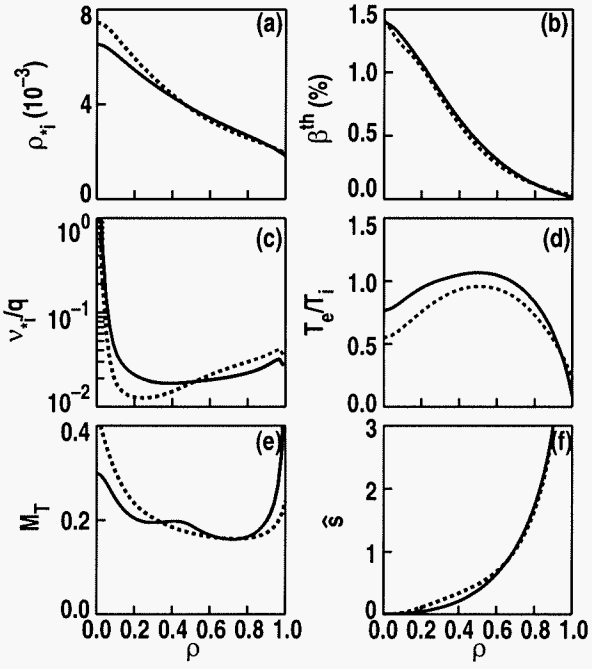

Fig. 4. Radial profiles of (a) relative ion gyroradius, (b) thermal beta, (c) ion collisionality, (d) ratio of electron-to-ion temperature, (e) toroidal Mach number, and (f) magnetic shear for the 0.8 MA (dashed lines) and 1.5 MA (solid lines) L-mode discharges.

uses the measured profiles of the electron density, electron and ion temperatures, ion toroidal rotation, effective ion charge, and radiated power. The radial heat flux is assumed to be purely diffusive in this analysis. The ratio of the effective (or one-fluid) thermal diffusivities for the low-q and high-q L-mode discharges of Table I is shown in Fig. 5, where the effective thermal diffusivity is defined by

$$\chi_{\text{eff}} = \frac{n_e \chi_e + n_i \chi_i}{n_e + n_i} \quad . \tag{4}$$

The uncertainty in the transport analysis displayed in Fig. 5 is due to random errors in the plasma profile measurements (the effect of potential systematic errors is small for this experiment). Using Eq. (2), the safety factor scaling of the effective thermal diffusivity is found to be approximately $\chi_{\text{eff}} \propto q^{0.84}$ with a random error of 0.15 in the q scaling exponent. The relatively weak q scaling of energy transport near the plasma edge appears to be in disagreement with models of the resistive ballooning mode [28] (predicted to be important only in the plasma edge) that have a robust transport scaling like $\chi \propto q^2$.

A two-fluid transport analysis finds that the ion thermal diffusivity has a stronger scaling with safety factor than does the electron thermal diffusivity in the outer regions of the plasma. This is demonstrated in Fig. 6, which shows the change in the ion and electron thermal diffusivities for the L-mode safety factor scan. The q scaling of the ion transport becomes stronger with increasing ρ, and has an average value of $\alpha_q = 0.9$ with a random error of 0.2. Conversely, the electron transport exhibits a weaker q scaling with increasing ρ, and has an average value of $\alpha_q = 0.7$ with a random error of 0.3. The larger error bars in Fig. 6 compared to Fig. 5 are due to the uncertainty in the electron-ion collisional energy exchange. The stronger q dependence displayed by ion energy transport compared to electron energy transport in the outer half of the plasma has also been found for H-mode plasmas on DIII-D [24].

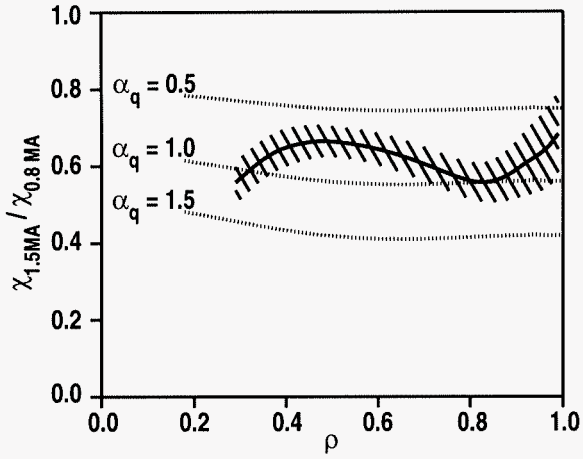

Fig. 5. Ratio of effective thermal diffusivities for the 1.5 MA and 0.8 MA L-mode plasmas with fixed magnetic shear as a function of normalized radius. The shaded region indicates the standard deviation of the random error.

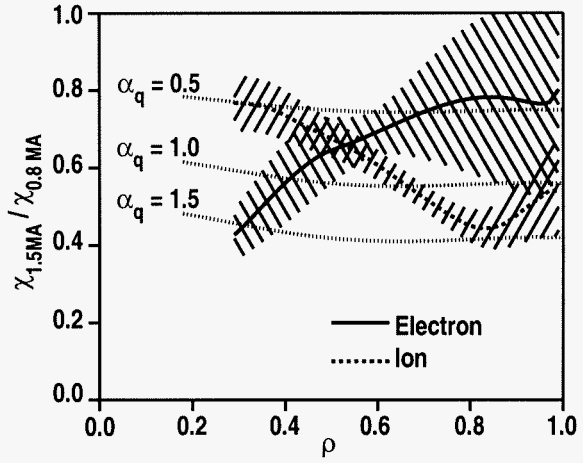

Fig. 6. Ratio of ion (dashed line) and electron (solid line) thermal diffusivities as a function of normalized radius for the 1.5 MA and 0.8 MA L-mode plasmas with fixed magnetic shear. The shaded regions indicate the standard deviation of the random error.

IV. THEORY-BASED TRANSPORT MODELING

In this section, the safety factor scans discussed in Sec. III and in Ref. [24] are simulated using the gyroLandau-fluid GLF23 transport model [27]. The GLF23 transport model is a one-dimensional (1D) dispersion type drift wave model with equations reduced from three-dimensional (3D) gyroLandau-fluid equations [40]. The 1D dispersion equations are fitted to the approximate linear growth rates from a 3D gyrokinetic stability (GKS) code, and the nonlinear saturation levels are taken from 3D gyroLandau-fluid simulations. The GLF23 transport model includes the effects of T_i/T_e, finite β (not included in these simulations), magnetic shear, Shafranov shift, and $E \times B$ shear stabilization. Neoclassical transport is also included in the modeling and is important in regions where turbulent transport is suppressed (such as near the plasma center). Recently, the GLF23 model was retuned to fit the linear growth rates for reversed magnetic shear parameters using the GKS code. The saturation levels were then normalized using nonlinear GYRO simulations [41] of the ITG mode assuming adiabatic electrons.

The ion temperature profiles are well simulated by the GLF23 transport model for the L-mode safety factor scan, as seen in Fig. 7, while the simulated electron temperature profiles are systematically too low by $\approx$15% in the core. In the GLF23 model, the density and toroidal velocity profile are taken from experiment, the poloidal velocity profile (which gives only a small contribution to the $E \times B$ velocity shear) is calculated from neoclassical theory, and the T_i and T_e profiles are simulated using the calculated radial heat fluxes from ohmic and NBI heating. Boundary conditions for T_i and T_e taken from the experiment are enforced at $\rho = 0.9$. The GLF23 transport model predicts that the dominant instability for ions is the ITG mode [42,43], while the electron temperature gradient (ETG) mode [44] is important for electrons in the plasma core.

Simulations using the GLF23 transport model predict a safety factor scaling of the energy transport that is close to (but slightly stronger than) the experimental observations for L-mode plasmas. The change in the ion and electron thermal diffusivities as modeled by GLF23 are shown in Fig. 8 for the q scan discussed in Sec. III. Theoretically, the toroidal ITG mode and trapped electron mode exhibit an approximately linear increase in transport with increasing safety factor, owing to the combined effects of a downshift of the spectral weight to long perpendicular wavelengths and a change in the turbulence growth rates [27]. This theoretical expectation is borne out in the GLF23 simulations shown in Fig. 8, where the predicted safety factor scaling of χ_e varies from $\alpha_q = 1.5$ near the plasma center to $\alpha_q = 0.5$ near the plasma edge,

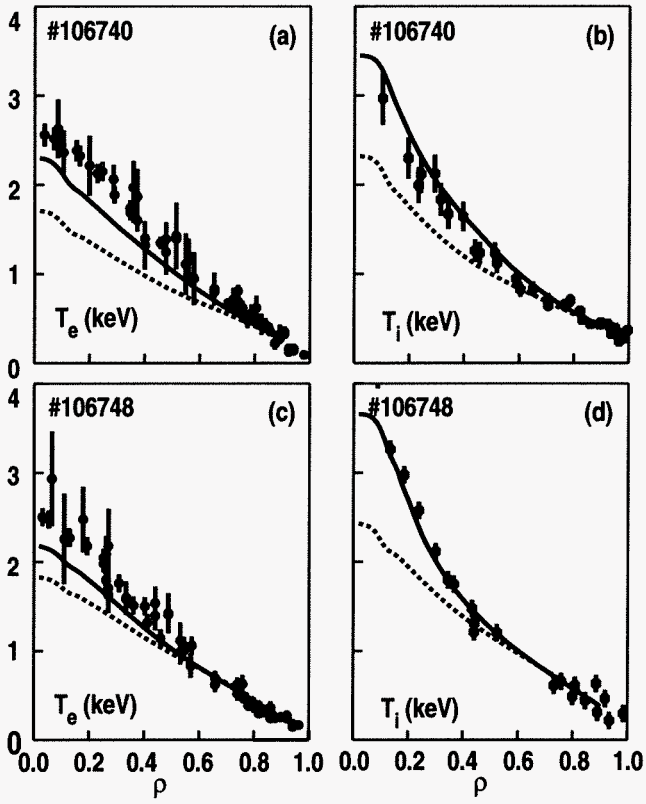

Fig. 7. Comparison of temperature profiles from experiment (circles and squares) and the GLF23 transport model with (solid lines) and without (dashed lines) $E\times B$ shear and Shafranov shift stabilization turned on for (a) electrons and (b) ions in the low-q discharge, as well as (c) electrons and (d) ions in the high-q discharge.

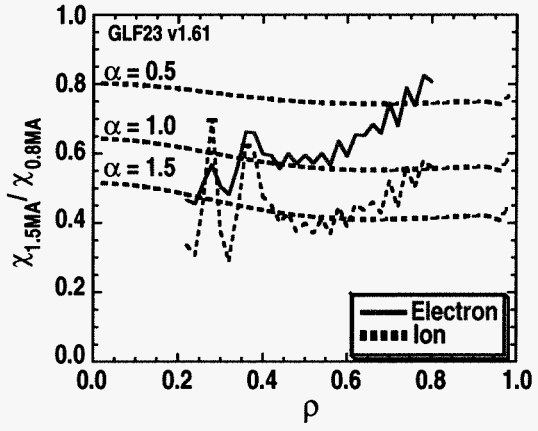

Fig. 8. Ratio of ion (dashed line) and electron (solid line) simulated thermal diffusivities as a function of normalized radius from the GLF23 transport model, including the effects of $E\times B$ shear and Shafranov shift stabilization, for the 1.5 MA and 0.8 MA L-mode plasmas.

in good agreement with the experimental results shown in Fig. 6. The agreement between simulation and experiment is not as good for χ_i, but the GLF23 modeling predicts that the ions should have a stronger q scaling than the electrons for $\rho > 0.4$, which agrees with the measured results shown in Fig. 6 for the outer half of the plasma.

Further examination of the GLF23 transport simulations finds that the scaling of the thermal diffusivities with safety factor shown in Fig. 8 is partially due to the effect of $E \times B$ shear stabilization. The toroidal Mach number is held constant during the q scan by adjusting the momentum injection from the neutral beams by selecting between two different toroidal injection angles. According to Eq. (3), the normalized $E \times B$ velocity shearing rate should decrease with increasing q at fixed M_T. Therefore, the effect of including $E \times B$ shear in the GLF23 transport simulations should be to strengthen the apparent q scaling of energy transport. Figure 7 shows that turning off the $E \times B$ shear and Shafranov shift stabilization in the GLF23 transport model results in significantly lower predicted electron and ion temperatures that are in worse agreement with experiment. This difference is mainly due to the $E \times B$ shear; the Shafranov shift is predicted to be a weak effect for all cases and is only slightly destabilizing owing to the positive magnetic shear profile. The $E \times B$ shear affects transport inside of $\rho = 0.5$ for the high-q case and inside of $\rho = 0.7$ for the low-q case. As a result, turning off the $E \times B$ shear and Shafranov shift stabilization in the GLF23 modeling gives a weaker predicted q scaling of energy transport for both the electron and ion channels, especially for $\rho \geq 0.5$, as shown in Fig. 9. Overall, it is clear the the simulated temperature profiles and simulated q scaling of the thermal diffusivities are in better agreement with experiment when the effects of $E \times B$ shear stabilization are included in the theory-based transport modeling.

Finally, the GLF23 transport model has been used to simulate the safety factor scaling of H-mode plasmas studied previously on DIII-D. These earlier experiments showed that the effective (or one-fluid) thermal diffusivity scaled like $\chi_{\text{eff}} \propto q^{2.3 \pm 0.6}$ at fixed magnetic shear for H-mode plasmas [24]. Figure 10 shows that the simulated q scaling of the effective thermal diffusivity by the GLF23 transport model for these H-mode discharges is in good agreement with the experimental result. Turning off $E \times B$ shear and Shafranov shift stabilization in the GLF23 model weakens the predicted q dependence, as seen in Fig. 10, similar to the L-mode case. The differences in the q scaling of H-mode and L-mode transport is not due to differences in the edge pedestal scalings since the β profiles are kept fixed in these experiments by adjusting the heating power. The stronger q scaling for H-mode, compared to L-mode, plasmas is apparently a consequence of H-mode plasmas having temperature

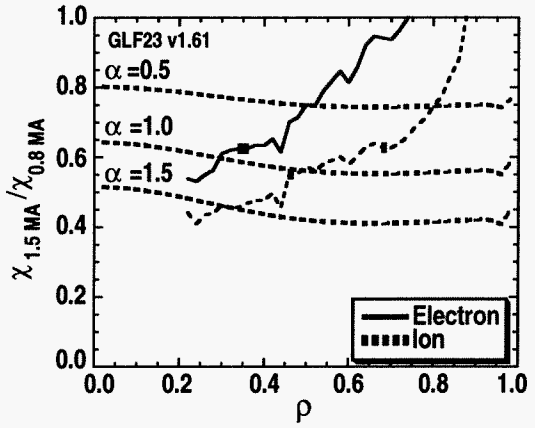

Fig. 9. Ratio of ion (dashed line) and electron (solid line) simulated thermal diffusivities as a function of normalized radius from the GLF23 transport model, not including the effects of $E\times B$ shear and Shafranov shift stabilization, for the 1.5 MA and 0.8 MA L-mode plasmas.

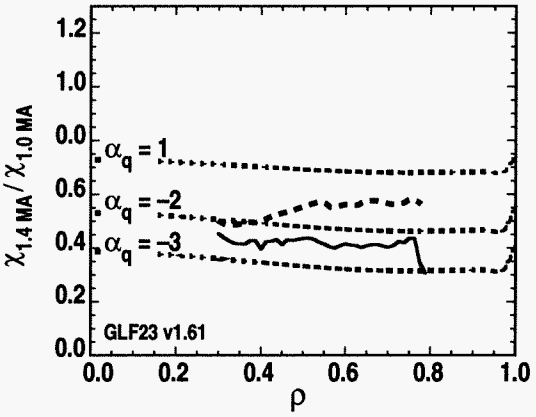

Fig. 10. Simulated ratio of the effective thermal diffusivities as a function of normalized radius from the GLF23 transport model, with (solid line) and without (dashed line) the effects of $E\times B$ shear and Shafranov shift stabilization, for the 1.4 MA and 1.0 MA H-mode plasmas discussed in Ref. [24].

gradients that are closer to marginal stability. The critical temperature gradient increases with lower q for both the ITG [45] and ETG [46] modes. Experiments on the Tore Supra tokamak [47] showed that the measured critical gradient using the electron temperature profile had a dependence like $\hat{s}/q$ [48]. Since for H-mode plasmas the temperature gradient is usually close to marginal stability [49], the change in the critical temperature gradient with q should strengthen the apparent q scaling of energy transport. On the other hand, for L-mode plasmas the temperature gradient is usually significantly greater than the critical gradient over a large region of the plasma [49], so changes in the critical temperature gradient with q will not be as important and the nearly linear q scaling of drift wave turbulence should prevail. Thus, the q dependence of the critical temperature gradient can explain the weaker q scaling of energy transport for L-mode (compared to H-mode) plasmas that is found both experimentally and in theory-based transport modeling.

V. COMPARISON OF DIMENSIONLESS AND PHYSICAL PARAMETER SCALINGS

Combining together the ρ_*, β, ν, and q scalings determined from separate experiments on DIII-D allows the dimensionless parameter scalings of L-mode plasmas to be compared with the physical parameter scalings empirically derived from multi-machine global confinement databases. This can help identify the underlying mechanisms of anomalous transport that are responsible for the observed physical parameter scalings (*i.e.*, I, B_T, *etc.*) of energy confinement. Experiments on DIII-D have shown that the beta scaling of the energy confinement time for L-mode plasmas is weak, possibly non-existent [21], while the collisionality scaling is also close to zero [22]. For L-mode plasmas, the relative gyroradius scaling of global confinement does not have a unique value because the ρ_* scalings of the electron and ion thermal diffusivities are not the same [11,12,50–52]. However, for the typical case of approximately equal ion and electron heat conduction, the energy confinement time exhibits Bohm-like scaling [11]. Assuming a power law form for the scaling relation, the dimensionless parameter scalings studies for L-mode plasmas on DIII-D can be summarized as

$$B_T \tau_{th} \propto \rho_*^{-2} \beta^{0.05 \pm 0.10} \nu^{0.02 \pm 0.03} q^{-0.8 \pm 0.1} \quad , \tag{5}$$

where the safety factor scaling from Sec. III is utilized. Sufficient information is contained in Eq. (5) to convert this global confinement scaling relation from dimensionless variables to physical variables by means of a straightforward algebraic manipulation,

$$\tau_{th} \propto I^{0.4} B_T^{0.1} n^{0.5} P^{-0.5} L^{2.1} \quad , \tag{6}$$

where L represents the physical size scaling (*i.e.*, a, R, *etc.*) needed to make the scaling relation dimensionally correct. Thus, it can be seen that the dimensionless parameter scaling approach yields a definitive prediction for the size scaling of confinement from single machine experiments.

It is interesting to compare Eq. (6) to the global confinement scaling relations that are derived from regression analysis of multi-machine confinement databases. For example, a commonly-used L-mode energy confinement scaling is the ITER-89P relation [53],

$$\tau_{89\mathrm{P}} = 0.048 I^{0.85} B_T^{0.2} n_{20}^{0.1} P^{-0.5} R^{1.5} \epsilon^{0.3} M^{0.5} \kappa^{0.5} \quad , \tag{7}$$

where M is the ion mass in AMU. The International Thermonuclear Experimental Reactor (ITER) [54] project has also recently determined a thermal energy confinement scaling that is nearly dimensionally correct [55],

$$\tau_{\mathrm{E,th}}^{\mathrm{L}} = 0.023 I^{0.96} B_T^{0.03} n_{19}^{0.40} P^{-0.73} R^{1.83} \epsilon^{-0.06} M^{0.2} \kappa^{0.64} \quad . \tag{8}$$

The most apparent difference between Eq. (6) and these empirically-derived confinement scaling relations is the weaker I scaling in the former due to the almost linear q scaling of transport reported in Sec. III. The q scaling in Eq. (5) would need to be at least two times stronger to bring the dimensionless variable and physical variable confinement scaling relations into agreement. The scaling of the other physical quantities in Eq. (6) are in better agreement with the empirically-derived relations. For example, the weak B_T scaling that is ubiqitious to confinement scaling relations is reproduced in Eq. (6) by means of a strong cancellation between the B_T scalings contained in the ρ_* and q terms.

Since Sec. IV showed that the nearly linear scaling of confinement with safety factor measured in L-mode plasmas on DIII-D is in agreement with theory-based transport models, it is likely that the weaker than expected current scaling in Eq. (6) is due to a difference in the execution of this experiment compared to how I scans are normally done. For example, $\hat{s}$ is held constant during the q scan discussed in Sec. III, whereas in the usual plasma current scan $\hat{s}$ decreases as I increases because $q(0)$ is fixed to unity by sawteeth. However, this discrepancy seems to be in the wrong direction to explain the weaker than expected q scaling measured on DIII-D. A more likely explanation is systematic differences in the boundary conditions between the q scan discussed in this paper and a normal I scan. In Sec. III, the boundary densities and temperatures are purposefully held fixed during the q scan by adjusting the gas fueling and NBI power. On the other hand, plasma current scans are usually done while holding the NBI power constant, thus it is reasonable to expect that the boundary temperature and perhaps density will increase with increasing I. For stiff transport models, a correlation between the boundary temperature and the plasma current would have the effect of strengthing the apparent I dependence of the energy confinement time. This explanation is supported by the analysis of the energy confinement time in H-mode plasmas with edge localized modes (ELMs) using a two-term model [56], where the stored energy of the edge pedestal is found to increase with plasma current approximately like $W_{ped} \propto I^2$, resulting in a weaker than linear scaling of the stored energy of the core region with plasma current, $W_{core} \propto I^{0.45}$.

VI. CONCLUSIONS

Experiments on DIII-D find an almost linear scaling of energy transport with safety factor at all radii for L-mode plasmas. In these experiments, the safety factor is varied by a factor of 1.8 at fixed magnetic shear while the other dimensionless parameters such as ρ_*, β, ν, *etc.*, are kept constant by holding the density, temperature, and toroidal magnetic field strength constant. The measured thermal confinement time scales like $\tau_{th} \propto q^{-0.8\pm0.1}$, while the effective (one-fluid) thermal diffusivity exhibits a similar q dependence, $\chi_{\text{eff}} \propto q^{0.84\pm0.15}$. The ion energy transport has a stronger q scaling than the electron energy transport in the outer half of the plasma. This q scaling of energy transport is significantly weaker than previously reported for H-mode plasmas on DIII-D [24]. For completeness, it would be useful to repeat this experiment while holding constant a different set of dimensionless parameters (e.g., poloidal rather than toroidal) to confirm that the measured q scaling of energy transport is related to the results presented in this paper by a straightforward transformation of variables.

Theory based modeling using the retuned GLF23 transport model is in good agreement with the experimental scaling of L-mode energy transport with safety factor, including a stronger q scaling for the ion channel compared to the electron channel in the outer regions of the plasma. The approximately linear scaling of transport with q is expected for the ITG mode and trapped electron mode, coming from both a downshift of the spectral weight to long perpendicular wavelengths as well as a change in the turbulence growth rates. Theory based modeling also shows that the q scaling of the thermal diffusivities is expected to be stronger for H-mode plasmas, approximately as $\chi_{\text{eff}} \propto q^2$. This stronger scaling for H-mode plasmas is apparently due to the temperature profiles being closer to marginal stability. Since the critical temperature gradient increases with lower safety factor, this gives rise to a favorable q scaling of energy transport over and above the nearly linear dependence expected from drift wave turbulence.

In spite of the good agreement between the theoretical and experimental safety factor scaling of L-mode confinement, there remains a discrepancy between this moderate dependence and the stronger $\chi_{\text{eff}} \propto q^{2-3}$ scaling needed to explain the well known linear dependence of the energy confinement time on the plasma current. Perhaps the resolution to this issue is the fact that the boundary densities and temperatures are held fixed in the q scaling experiments reported here, whereas the multi-machine confinement database likely contains a strong correlation between I and the boundary temperature (and density) at fixed heating power. For stiff transport models, this correlation would result in a stronger I scaling of energy confinement than would

be predicted from the dimensionless parameter experiments discussed in this paper. Further studies need to be done to understand whether the boundary conditions or some other effect can reconcile the weaker q scaling of energy transport measured (and predicted) on DIII-D with the stronger scaling expected from empirically-derived confinement scaling relations.

REFERENCES

[1] B. B. Kadomtsev, Sov. J. Plasma Phys. **1**, 295 (1975).

[2] J. W. Connor and J. B. Taylor, Nucl. Fusion **17**, 1047 (1977).

[3] J. W. Connor, Plasma Phys. Control. Fusion **30**, 619 (1988).

[4] E. Buckingham, Phys. Rev. **4**, 345 (1914).

[5] T. C. Luce, C. C. Petty, J. G. Cordey *et al.*, Nucl. Fusion **42**, 1193 (2002).

[6] R. E. Waltz, J. C. DeBoo and M. N. Rosenbluth, Phys. Rev. Lett. **65**, 2390 (1990).

[7] J. P. Christiansen, P. M. Stubberfield, J. G. Cordey *et al.*, Nucl. Fusion **33**, 863 (1993).

[8] F. W. Perkins, C. W. Barnes, D. W. Johnson *et al.*, Phys. Fluids B **5**, 477 (1993).

[9] U. Stroth, G. Kühner, H. Maassberg, H. Ringler and the W7-AS Team, Phys. Rev. Lett. **70**, 936 (1993).

[10] J. B. Wilgen, M. Murakami, J. H. Harris *et al.*, Phys. Fluids B **5**, 2513 (1993).

[11] C. C. Petty, T. C. Luce, R. I. Pinsker *et al.*, Phys. Rev. Lett. **74**, 1763 (1995).

[12] C. C. Petty, T. C. Luce, K. H. Burrell *et al.*, Phys. Plasmas **2**, 2342 (1995).

[13] H. Shirai *et al.*, J. Phys. Soc. Japan **64**, 4209 (1995).

[14] J. G. Cordey, B. Balet, D. Campbell *et al.*, Plasma Phys. Control. Fusion **38**, A67 (1996).

[15] F. Ryter, M. Alexander, O. Gruber, *et al.*, in *Plasma Physics and Controlled Nuclear Fusion Research*, Montreal, 1996, (International Atomic Energy Agency, Vienna, 1997), Vol. 1, p. 625.

[16] M. Greenwald, J. Schachter, W. Dorland *et al.*, Plasma Phys. Control. Fusion **40**, 789 (1998).

[17] H. Shirai, T. Takizuka, Y. Koide *et al.*, Plasma Phys. Control. Fusion **42**, 1193 (2000).

[18] C. C. Petty, M. R. Wade, J. E. Kinsey, D. R. Baker, and T. C. Luce, Phys. Plasmas **9**, 128 (2002).

[19] S. D. Scott, C. W. Barnes, D. R. Mikkelsen *et al.*, in *Plasma Physics and Con-*

trolled Nuclear Fusion Research, Würzburg, 1992, (International Atomic Energy Agency, Vienna, 1993), Vol. 3, p. 427.

[20] JET Team, presented by J. G. Cordey, in *Plasma Physics and Controlled Nuclear Fusion Research*, Montreal, 1996, (International Atomic Energy Agency, Vienna, 1997), Vol. 1, p. 603.

[21] C. C. Petty, T. C. Luce, J. C. DeBoo, R. E. Waltz, D. R. Baker, and M. R. Wade, Nucl. Fusion **38**, 1183 (1998).

[22] C. C. Petty and T. C. Luce, Phys. Plasmas **6**, 909 (1999).

[23] J. L. Luxon, Nucl. Fusion **42**, 614 (2002).

[24] C. C. Petty, T. C. Luce, D. R. Baker *et al.*, Phys. Plasmas **5**, 1695 (1998).

[25] M. Ottaviani and G. Manfredi, Nucl. Fusion **41**, 637 (2001).

[26] J. W. Connor and H. R. Wilson, Plasma Phys. Control. Fusion **36**, 719 (1994).

[27] R. E. Waltz, G. M. Staebler, W. Dorland, G. W. Hammett, M. Kotschenreuther and J. A. Konings, Phys. Plasmas **4**, 2482 (1997).

[28] D. R. McCarthy, P. N. Guzdar, J. F. Drake, T. M. Antonsen, Jr., and A. B. Hassam, Phys. Fluids B **4**, 1846 (1992).

[29] T. N. Carlstrom, G. L. Campbell, J. C. DeBoo, R. Evanko and J. Evans, Rev. Sci. Instrum. **63**, 4901 (1992).

[30] M. E. Austin, R. F. Ellis, J. L. Doane and R. A. James, Rev. Sci. Instrum. **68**, 480 (1997).

[31] P. Gohil, K. H. Burrell, R. J. Groebner and R. P. Seraydarian, Rev. Sci. Instrum. **61**, 2949 (1990).

[32] M. R. Wade, D. L. Hillis, J. T. Hogan *et al.*, Phys. Plasmas **2**, 2357 (1995).

[33] A. W. Leonard, W. H. Meyer, B. Geer, D. M. Behne and D. N. Hill, Rev. Sci. Instrum. **66**, 1201 (1995).

[34] L. L. Lao, J. R. Ferron, R. J. Groebner *et al.*, Nucl. Fusion **30**, 1035 (1990).

[35] D. Wróblewski and L. L. Lao, Rev. Sci. Instrum. **63**, 5140 (1992).

[36] B. W. Rice, K. H. Burrell, L. L. Lao, and Y. R. Lin-Liu, Phys. Rev. Lett. **79**, 2694 (1997).

[37] B. W. Rice, T. S. Taylor, K. H. Burrell *et al.*, Plasma Phys. Control. Fusion **38**, 869 (1996).

[38] T. L. Rhodes, J.-N. Leboeuf, R. D. Sydora *et al.*, Phys. Plasmas **9**, 2141 (2002).

[39] H. St. John, T. S. Taylor, Y.-R. Lin-Liu and A. D. Turnbull, in *Plasma Physics and Controlled Nuclear Fusion Research*, Seville, 1994 (International Atomic Energy Agency, Vienna, 1995), Vol. 3, p. 603.

[40] R. E. Waltz, G. D. Kerbel, and J. Milovich, Phys. Plasmas **1**, 2229 (1994).

[41] J. Candy and R. E. Waltz, Journal of Computational Physics **186**, 545 (2003).

[42] W. M. Tang, G. Rewoldt, and L. Chen, Phys. Fluids **29**, 3715 (1986).

[43] R. R. Dominguez and R. E. Waltz, Phys. Fluids **31**, 3147 (1988).

[44] F. Jenko, W. Dorland, M. Kotschenreuther, and B. N. Rogers, Phys. Plasmas **7**, 1904 (2000).

[45] W. Dorland, M. Kotschenreuter, M. Beer, *et al.*, in *Plasma Physics and Controlled Nuclear Fusion Research*, Seville, 1994 (International Atomic Energy Agency, Vienna, 1995), Vol. 3, p. 463.

[46] F. Jenko, W. Dorland, and G. W. Hammett, Phys. Plasmas **8**, 4096 (2001).

[47] Equipe Tore Supra, presented by R. Aymar, in *Plasma Physics and Controlled Nuclear Fusion Research*, Nice, 1988, (International Atomic Energy Agency, Vienna, 1989), Vol. 1, p. 9.

[48] G. T. Hoang, C. Bourdelle, X. Garbet *et al.*, Phys. Rev. Lett. **87**, 125001 (2001).

[49] D. R. Baker, G. M. Staebler, C. C. Petty, C. M. Greenfield, and T. C. Luce, Phys. Plasmas **10**, 4419 (2003).

[50] T. C. Luce and C. C. Petty, in *Proceedings of the 22nd European Conference Controlled Fusion and Plasma Physics, Bournemouth, 1995* (European Physical Society, Geneva, 1995), Vol. 19C, Part III, p. 25.

[51] D. R. Baker, M. R. Wade, L. Y. Sun, C. C. Petty, and T. C. Luce, Nucl. Fusion **40**, 799 (2000).

[52] G. R. McKee, C. C. Petty, R. E. Waltz *et al.*, Nucl. Fusion **41**, 1235 (2001).

[53] P. N. Yushmanov, T. Takizuka, K. S. Riedel *et al.*, Nucl. Fusion **30**, 1999 (1990).

[54] R. Aymar, Plasma Phys. Contr. Fusion **42**, B385 (2000).

[55] ITER Physics Basis, Nucl. Fusion **39**, 2175 (1999).

[56] K. Thomsen, J. G. Cordey, *et al.*, Plasma Phys. and Control. Fusion **44**, A429 (2002).

ACKNOWLEDGMENTS

This work is supported by the U.S. Department of Energy under Contract No. DE-AC03-99ER54463 and Grant No. DE-FG02-92ER54141. We thank T.L. Rhodes for leading this experiment and R.E. Waltz for useful discussions on this subject.